Nanoscale

Accepted Manuscript

This article can be cited before page numbers have been issued, to do this please use: J. S. Barnard, C. Paukner and K. Koziol, *Nanoscale*, 2016, DOI: 10.1039/C6NR03895F.

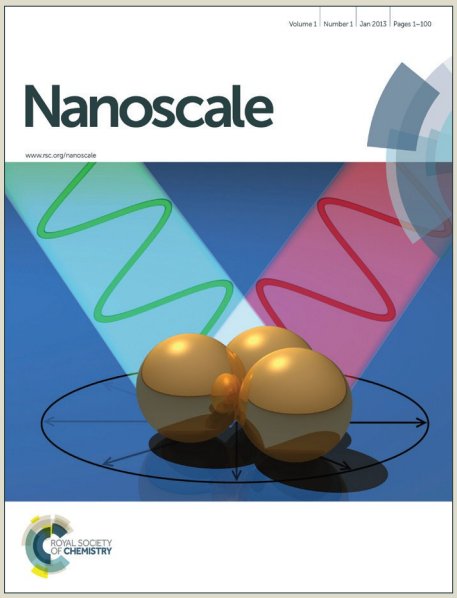

ROYAL SOCIETY OF CHEMISTRY

www.rsc.org/nanoscale

View Article Online
DOI: 10.1039/C6NR03895F

Nanoscale

RSCPublishing

ARTICLE

The role of carbon precursor on carbon nanotube chirality in floating catalytic chemical vapour deposition

Cite this: DOI: 10.1039/x0xx00000x

J. S. Barnard[a], C. Paukner[a] and K.K. Koziol[a]

Received ooth January 2015,
Accepted ooth January 2015

DOI: 10.1039/x0xx00000x

www.rsc.org/

We have studied the influence of different carbon precursors (methane, ethanol and toluene) on the type, diameter and chiral angle distributions of carbon nanotubes (CNTs) grown with the floating catalyst technique in a horizontal gas-flow reactor. Using electron diffraction to study their atomic structures, we found that ethanol and toluene precursors gave high single-wall CNT yields (92% and 89% respectively), with narrow diameter distributions: 1.1 nm to 1.7 nm (ethanol); 1.3 nm to 2.1 nm (toluene), with a propensity for armchair-type chiral angles. In contrast, methane-grown CNTs gave high double-wall CNT yields (75%) with broader diameter populations: 1.2 to 4.6 nm (inner CNT) and 2.2 to 5.3 nm (outer CNT) with a more uniform spread of chiral angles, but weakly peaked around 15 to 20 degrees. These observations agree with known growth models. However, double-wall CNTs grown with toluene showed an unusually narrow interlayer spacing of 0.286±0.003 nm with suggestions of large, 20° to 25°, differences between inner and outer CNT chiral angles. Methane gave a large interlayer spacing (0.385±0.002 nm) with suggestions of small 5° to 10° inter-tube chirality correlations.

Introduction

Carbon nanotubes (CNTs) are hexagonal sheets of carbon atoms rolled into a tube with a diameter in the nanometre range. The atomic structure of a CNT is determined by its chirality, a pair of integers (*n,m*) that describe how to span the circumference of the tube using the 2-dimensional basis of lattice vectors of a planar sheet of carbon atoms. The chiral indices also determine the pseudo one dimensional 'unit cell' needed to extend the tube indefinitely[1,2]. Bar its length, the chirality defines the complete atomic structure of a CNT.

At present CNTs are typically grown with the catalytic chemical vapour deposition technique (CCVD) from decomposition of a hydrocarbon. This is pyrolysed, i.e. thermally decomposed in the absence of oxygen, and assembled into the tube with the aid of a carrier gas, either over a catalytically-loaded substrate, or, with the catalyst moving within the gas stream (floating CCVD)[3,4]. The role of the catalyst is not only to facilitate the decomposition of the precursors, but to provide a nanoscale template for the tube to nucleate and grow[5].

The high pressure carbon monoxide synthesis (HiPCO) developed by Richard Smalley's team at Rice University in the 1990s provided the first significant benchmark in CVD CNT synthesis[6,7]. The HiPCO synthesis disproportionates carbon monoxide, via the Boudouard mechanism, to drive carbon precipitation from the solid metal-organic precursors, $Fe(CO)_5$ and $Mo(CO)_5$, which acts as both catalyst and carbon source. Further improvement came when a gaseous carbon monoxide precursor and a solid Co-Mo bimetallic catalyst was used- the CoMoCAT synthesis set a new benchmark at the start of the 21st century, growing narrower SWNTs with small chirality distributions[8-11]. Chiral selectivity has since improved by, e.g. suppressing Ostwald ripening with higher melting temperatures and size-selecting the bimetallic catalysts using molecular clusters[12]. Further, by using an organic template or selectively purified CNTs, the catalyst can be eliminated altogether. For example, exclusively (6,6) armchair-type SWNTs have been grown using the polycyclic hydrocarbon $C_{96}H_{54}$ as an end-cap nucleating agent on a platinum (111) surface[13] and CNTs have been selectively purified and cloned on a quartz surface without the need of a catalyst[14]. However, all of these developments have been confined to substrate-bound catalysing/nucleating agents, which limit the scalability needed for industrial quantities of CNTs. The challenge remains to grow single chirality CNTs with the floating CCVD method.

The structure-growth relationship of CNTs has been extensively studied ever since the discovery of CVD growth of fibers in 1973[15] and few-wall CNTs in 1991[16]. In their review in 2007, Lamouroux, Serp & Kalck suggested that the five principle properties that affect CNT growth are catalyst composition, catalyst size, temperature, gas chemistry and carbon source gas partial pressure[17]. Nickel, iron and cobalt are now commonly known to be effective catalysts in that order[5].

View Article Online
DOI: 10.1039/C6NR03893F

The catalyst nucleates a CNT with a diameter that is slightly smaller than the catalyst size, as seen in both post-growth material[7,18,19], and *in-situ* growth in environmental transmission electron microscopes[20-22]. The optimal growth temperature appears to lie between 700 and 1200 °C, i.e. between amorphous carbon formation at low temperature and graphitisation at high temperature[17,23,24]. However, the exact temperature is very sensitive to the specific growth system. Less agreement exists on the role of gas chemistry, but many hydrocarbons including saturated, e.g. methane[25,26], and unsaturated hydrocarbons, e.g. ethyne[9], alcohol[27], benzene[28] and aromatic alcohols (phenols) are now known to produce CNTs[5]. Several studies have examined the role of carbon precursor explicitly, comparing, for example, carbon monoxide and methane[29]; carbon monoxide, ethanol, methanol and ethyne[9]. More recently, He *et al* have examined structural differences between CO and methane grown tubes using electron diffraction methods[30].

In a similar manner to He *et al*, our aim with this survey was to explore, in detail, how the choice of carbon precursor affected the nature of CNTs grown in a floating CCVD reactor at atmospheric pressure (100 kPa). Much of the early work to optimise the growth conditions for producing a continuously spun CNT fibre, using Raman spectroscopy, was reported earlier[31]. This detailed survey was warranted because of the sensitivity offered by electron diffraction to the atomic structure of a CNT, in particular, its chirality[32,33].

Experimental Methods

CNT synthesis

Carbon nanotubes were grown in a horizontally mounted version of the reactor reported earlier[31]. This solved the problem of turbulent convective mixing caused by dropping cool gases into a hot reactor tube. In all other respects the reactor was the same.

The furnace temperature was 1200°C and heated over a length of 80 cm (Figure 1). The temperature gradient at the entrance of the furnace was 55°C cm^{-1}, and was measured with a moveable thermocouple.

Three injectors were placed at the front of the reactor to deliver the hydrogen carrier gas, ferrocene and the hydrocarbon source(s). The carrier gas was supplied at a rate of 2000 standard cubic centimetres per minute (sccm) with no pre-heating, i.e. the hydrogen gas cylinder remained at room temperature. Table 1 summarizes the source, injection and pyrolysis temperatures, the measured molar flow rates and helium volume flow for transporting non-gaseous sources into the reactor that were typically used for growth. The estimated Reynolds number was Re ~ 0.5, which corresponds to creeping fluid flow. No hetero-atomic promoters were used and the growth conditions were identical for all carbon precursors.

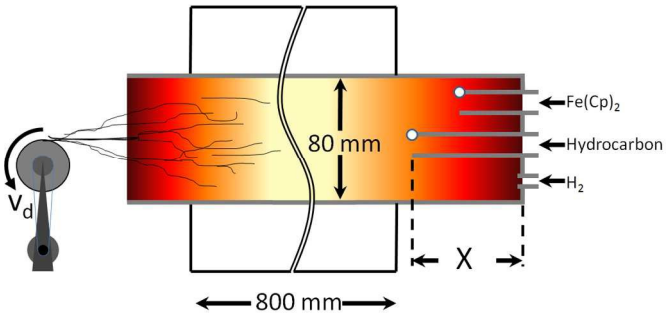

Figure 1. The reactor and injector geometry used here for CNT growth. Ferrocene, "$Fe(Cp)_2$", and carbon precursors, "hydrocarbon", were fed by ¼-inch stainless steel tubes mounted with K-type Alumel-Chromel thermocouples (white dots) at their exit orifices. The ferrocene injector was fixed, but the hydrocarbon injector had a *moveable* injector distance, *X*, from the end flange. Hydrogen was fed with a ⅛-inch stainless steel injector. CNTs were drawn out of the reactor at a velocity, v_d, that varied from 10 m/min (slow growth) to 50m/min (fast growth). The colour grading represents the reactor temperature and is for illustrative purposes only.

The location of the specific hydrocarbon injector, X in figure 1, was optimised to obtain clean, small diameter CNTs as measured by Raman spectroscopy (see Supplementary Information). We used the intensity ratios D:G and 2D:G, of the Raman G (1589 cm^{-1}), D (1300 cm^{-1}) and 2D (2600 cm^{-1}) peaks to optimize the hydrocarbon injector position in the reactor. Electron diffraction was employed after the Raman optimization process. Details of the growth process have been published elsewhere[31].

Table 1 The temperatures used for the containing vessels (T_{source}), the furnace injection points (T_{inject}) and the pyrolysis (T_{pyro}). Calibrated molar flow rates and range of helium (volume) flow rate used to carry non-gaseous sources into the reactor.

	$Fe(Cp)_2$	Carbon precursors		
		C_2H_5OH	CH_4	C_7H_7
T_{source} (°C)	70	50	25	50
T_{inject} (°C)	280	550	550	450
T_{pyro} (°C)	400	~750	~1200	~780
Flow (mmol min^{-1})	0.002	1.5	1.6	0.8
He flow (sccm)	100-200	50-200	0	30-100

TEM sample preparation

Diffraction of CNTs requires individual tubes to be well dispersed on the TEM grid. Attempts with liquids proved ineffectual. Organic solvents like ethanol, toluene and N-methyl-2-pyrrolidone preferentially dissolved impurities, which reappeared upon evaporation as a concentrated powder mingled with the tubes. Water dispersal gave a slimy residue owing to surfactants used in the process, which covered all the tubes in an amorphous film. Very few CNTs fit for diffraction analysis resulted. Instead, we used mechanical methods (scraping) to mount the tubes onto empty copper grids (Figure 2) or copper grids with holey carbon film. A holey carbon film provided

Journal Name

View Article Online
DOI: 10.1039/C6NR06895F

mechanical support, which reduced CNT movement and image blur. Scraping the CNTs also reduced the risk of contamination.

TEM analysis

All the carbon nanotubes were analysed using an FEI Tecnai Osiris TEM operated at 80 kV, i.e. below the knock-on damage threshold[34]. We used a two-step process to find the individual tubes and obtain their diffraction patterns. First, bright-field (BF) images were used to identify and locate the isolated tubes against a backdrop of CNT bundles, iron particles and carbon support film (Figures 2 and 3). CNTs were distinguishable by their empty interiors. Second, a small (9 nm FWHM), highly collimated (0.23 mrad semi-angle) probe carrying 2.43 pA was formed and we returned to each tube and collected a 10 second exposure on a Gatan UltraScan 1000XP slow-scan camera, i.e. about 150 million electrons per diffraction pattern (significant scope exists to reduce this). No spot fading was seen, suggesting that the integrity of the CNT was maintained throughout. Every experiment was calibrated against diffraction patterns from polycrystalline gold films. We aimed for a target of between 50 and 150 tubes for each sample for a statistically significant analysis.

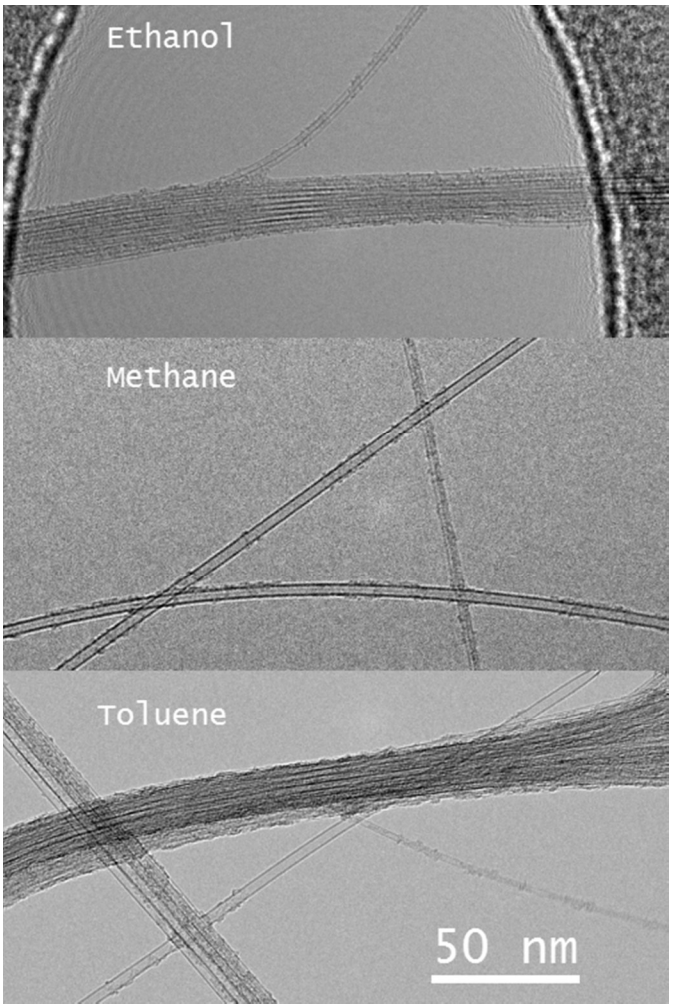

Figure 2. Bright-field images of single tubes and the associated bundles from the three hydrocarbon precursors. Part of the holey (amorphous) carbon support film can be seen for the ethanol-grown tubes.

Every diffraction pattern was analysed to extract three properties (Figure 3): the nature of the tube, i.e. single-wall (SWNT), double-wall (DWNT) or multi-wall (MWNT); the tube diameter(s) using the periodicities inherent in the equatorial diffraction fringes; the chiral angle of the weaker Bessel fringes associated with the twisted graphitic lattice[32]. These three properties were combined to return the tube type, its diameter and its chirality (*n,m*). Occasionally, multiple diffraction patterns from the same tube were taken to ensure measurement consistency. The process by which we identified individual tubes and acquired diffraction patterns is detailed in the Supplementary Information.

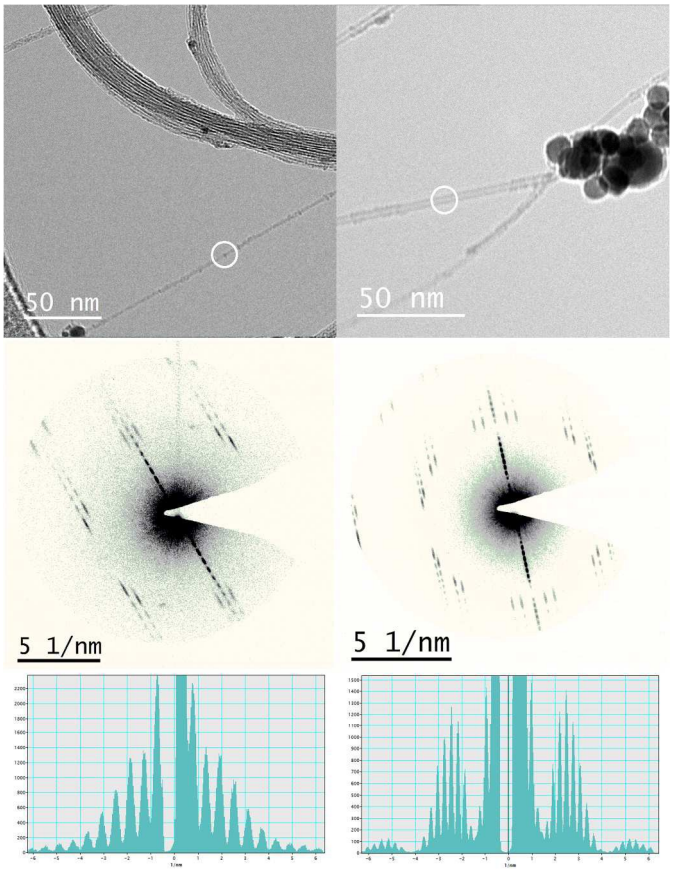

Figure 3. Exemplar images and diffraction patterns from a (14,11) SWNT (left) grown from an ethanol source and a (32,12)@(34,21) DWNT (right) from the methane source. The equatorial line intensity distributions (bottom) show how the narrow tubes lead to broad diffraction fringes and *vice versa*.

Results

Good, clean CNT fibres were achieved with all three carbon sources (Figure 2). Many of the tubes existed in bundles, e.g. top-left image in figure 3, but isolated tubes were always seen

View Article Online
DOI: 10.1039/C6NR03693F

emerging from the main bundle. Some CNTs had patches of thin amorphous material adsorbed on the outside. This gave rise to diffuse scattering (streaks and rings) in the diffraction pattern, but did not detract from the CNT diffraction features.

Figure 4 shows the population map of all the SWNTs and *inner* CNTs of DWNTs only. The population map of the outer CNTs is not shown here (see Supplementary Information). The total number for tubes analysed was 74 (ethanol), 77 (methane) and 152 (toluene). Only 6 out of 74 CNTs were identified as DWNTs for the ethanol-grown tubes (92% SWNT yield). 58 out of 77 CNTs were identified as DWNTs for methane-grown material (25% SWNT yield). For toluene, the DWNT count was 17 out of 152 tubes (89% SWNT yield). A small number of MWNTs

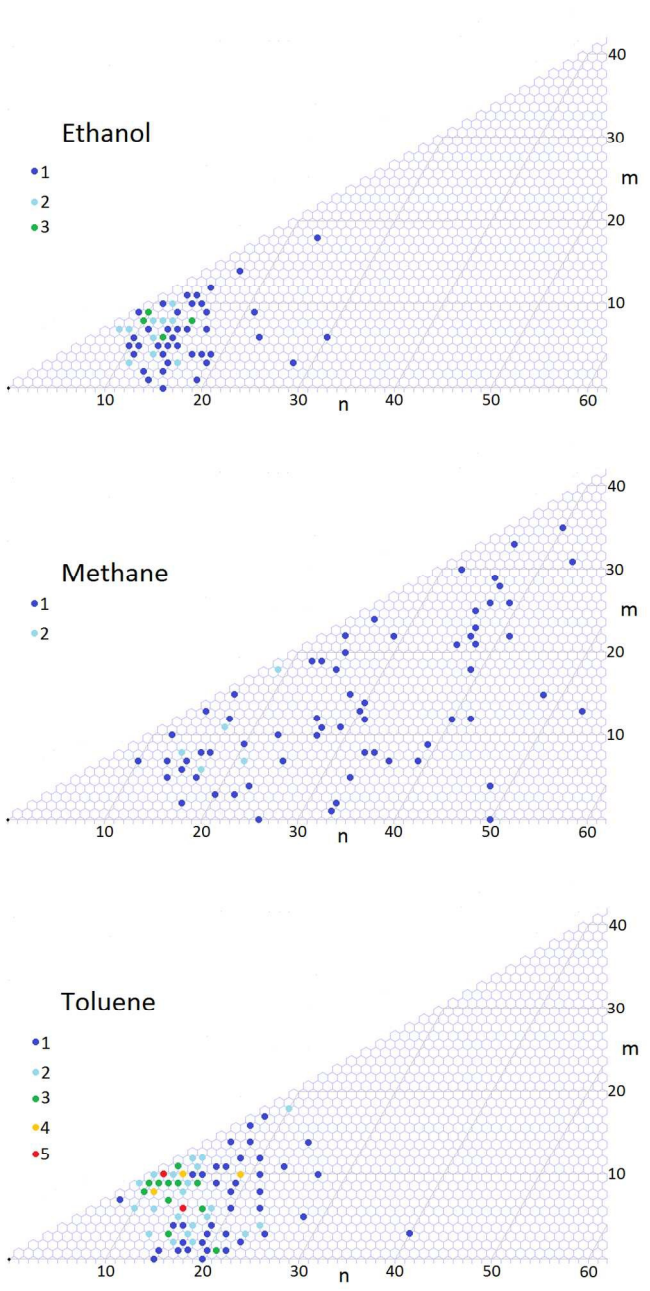

Figure 4. Chirality maps (on the irreducible wedge of hexagonal lattice orientations) for the inner & SWNTs only, with dots colour-coded according to frequency. The number of identifiable tubes on each map *is different*: N=74 (ethanol, top), N=77 (methane, middle) and N=152 (toluene, bottom).

were excluded from the count, which would suggest these percentages for SWNT yields are an upper limit.

Figure 5 summarizes the cumulative diameter distributions in which all tubes were assigned to their nearest 0.1 nm spaced bin. The narrowest distribution of inner/SWNTs was found for ethanol: 1.1 nm to 1.7 nm (10% to 90% population diameters), with more than half its tubes having a diameter of <1.4 nm. The peak population was at 1.2 nm (14 tubes, 18% of total). A few tubes were as large as 3 nm, e.g. the two tubes identified as (23,18) in Figure 4. The second narrowest distribution was the

View Article Online
DOI: 10.1039/C6NR03895F
ARTICLE

toluene-grown material: 1.3 nm to 2.1 nm (10% to 90%), i.e. about 0.2 nm wider than the ethanol material, but with a similarly shaped distribution. More than half the tubes had a diameter of <1.6 nm and the peak population level was 1.5 nm (27 tubes, 36% of total). A slightly wider tail in the toluene distribution accounted for the bigger 90% population diameter. The largest tubes were seen for the methane carbon source, which were at least twice the width of the ethanol tubes and had a very wide overall distribution: 1.6 nm to 4.6 nm (10 % to 90 %); more than half the tubes were <2.8 nm wide. The peak populations occurred at 1.6 nm, 2.1 nm and 2.7 nm (6 tubes per bin, or 8% for each).

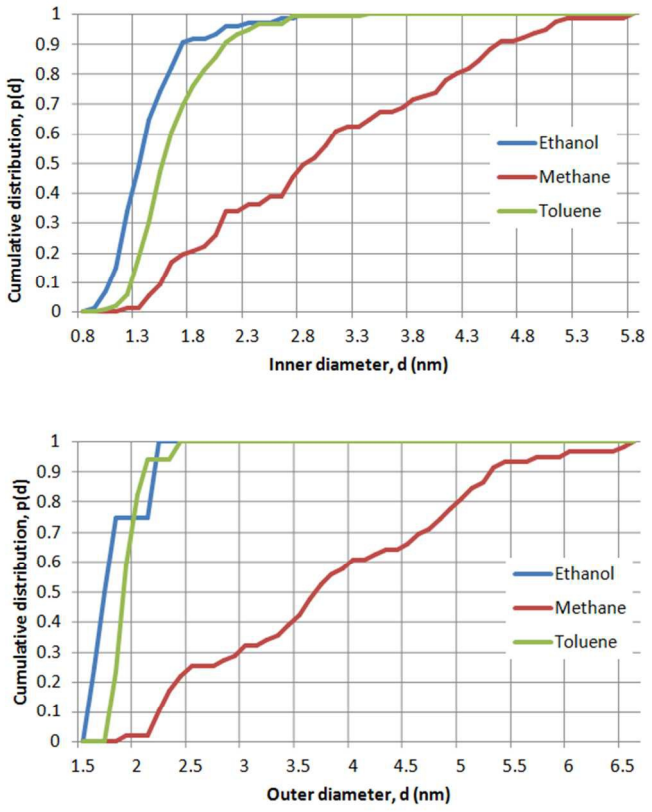

Figure 5. Cumulative diameter distributions for inner and SWNT tubes only (top): N=74 (ethanol), 77 (methane) & 152 (toluene). The outer diameter distribution for DWNTs only (bottom): N=4 (ethanol), 58 (methane) & 17 (toluene). Population distributions can be found in the Supplementary Information.

Like their inner counterparts, the diameter distributions for the (few) outer-tubes for ethanol were slightly smaller than for toluene at both the 10 % (1.6 nm & 1.8 nm) and 50 % populations (1.7 nm & 1.9 nm). The methane outer-tube population showed more structure than the inner-tube counterpart with three rises at approximately 2.2 nm, 3.6 nm and 4.8 nm (Figure 5, lower). These rises were more pronounced than the inner-tube distribution.

Both the ethanol and toluene grown SWNT and inner tubes had a propensity for armchair-like chiral arrangements (Figure 6). For ethanol, 28% of the tubes were within 5° of the armchair configuration compared to 4 % within the zig-zag one, a seven-fold variation. The toluene grown material was less skewed: 28% were within 5° of armchair and 9 % within 5° of the zig-zag chirality. The outer tubes for the few DWNTs found in these materials were found to be either predominantly armchair (ethanol) or zig-zag like for toluene.

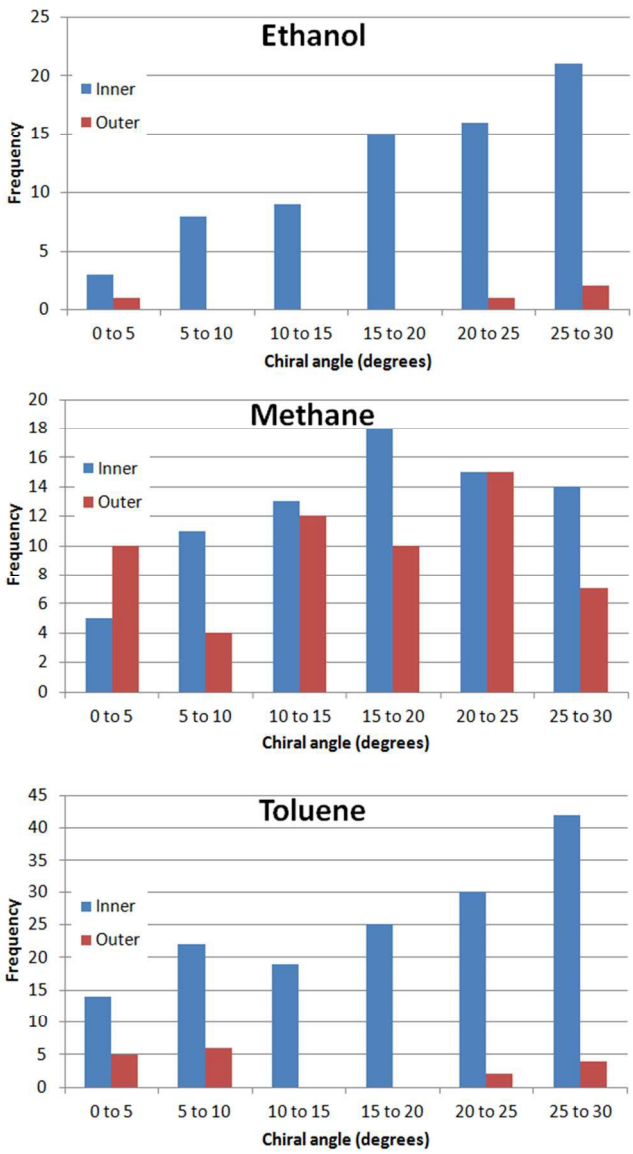

Figure 6. Inner and outer chiral angles of all three carbon sources. Both the SWNT and DWNT outer chirality are displayed.

The methane-sourced tubes, both inner and outer, had a more uniform chiral distribution with peak populations between 15° to 20° (inner) and 20° to 25° (outer).

Figure 7 shows the inter-tube chirality relationships for all the DWNTs that were identified in each sample. The inter-tube angle, $\Delta\alpha$, is that angle needed to bring the inner tube in line with the outer tube. A positive value means the outer tube is more arm-chair like than the inner tube and *vice versa*. The frequency plots show the measured frequencies (coloured bars,

View Article Online
DOI: 10.1039/C6NR03699F

labelled "Observed") for each 5° angular bin, relative to the expected mean for *randomly uncorrelated* tubes (grey bars, labelled "Theory"). If the tubes are correlated, then significant differences between the "Observed" and "Theory" bars should be seen, i.e. a large excess *or* deficit. With only four DWNTs seen for ethanol, no statistically meaningful observations could be made for this material.

With its higher number of DWNTs, methane showed two distinct excess peaks in the ±"5 to 10" angular bins, i.e. the outer tubes prefer to grow with a (±) 5° to 10° chiral angle differences. The statistical significances for these are 1.9σ (-5° to -10°) and 1.4σ (5° to 10°), which are suggestive.

The most (statistically) significant inter-tube chiral correlation was observed for toluene for a difference of -20° to -25° (2.1σ). There was no significant correlation in the opposite direction. This suggests that predominantly arm-chair like inner-tubes favours the growth of zig-zag like outer-tubes in the few cases that DWNT growth occurs (11% of the total).

The spacing between the inner and outer tubes for the DWNTs showed significant differences between the carbon sources. The inter-layer separation between inner and outer was 0.323±0.009 nm for ethanol, 0.384±0.002 nm for methane and 0.286±0.003 nm for toluene. This contrasts with the value for graphite of 0.334 nm.[2]

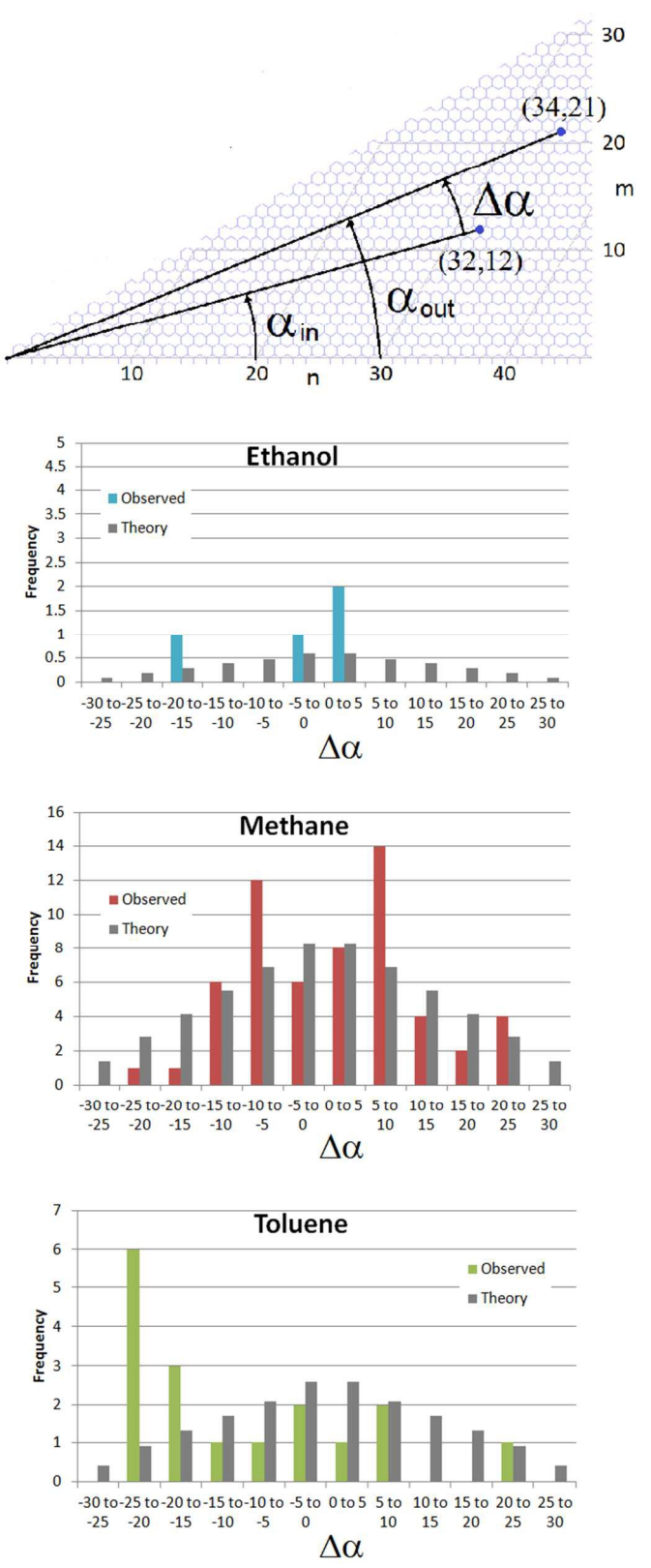

Figure 7. DWNT inter-tube angles using, for example, the DWNT in figure 2 (*32,12*)@(*34,21*). The inter-tube angles for ethanol show no difference, but methane and toluene show more significant correlations.

Journal Name

View Article Online
DOI: 10.1039/C6NR03895F

Discussion

How representative is an individual CNT?

Electron diffraction has been used to characterize CNTs in a number of studies[30,32,35,36]. Recovering the electron diffraction of a single tube within a bundle is a computationally demanding task, because the amplitude of each CNT is phased according to its position within the bundle and the problem becomes one of structural refinement (tube type and location)[37]. Individual tubes eliminate that task. However, this replaces a computational problem with a conceptual one – *how representative is an individual CNT?*

All the tubes we studied were seen close to, or emerging from, bundles of CNTs within several hundred nanometres (given their higher visibility, bundles were used to locate individual CNTs as part of our methodology; see Supporting Information). Given the long length of the CNT fibre, it is reasonable to assume that, with the snapshot in growth history recorded in our samples, individual tubes would have been nucleated and grown at times similar to those CNTs in bundles. It *is* conceivable that the bundled tubes shared their genesis on a single catalytic particle with the perpendicular growth mode, noted by Fiawoo *et al*[19]. However, this growth mode tends to stagnate and few tubes emerge beyond 10 nm in this configuration. It is more likely that the bundles we see are individual tubes that come into serendipitous contact during the motion within the hot carrier gas (and subsequent handling during collection and preparation) and are held together by van der Waals forces. However, any evidence of similarity between size distributions obtained by another technique, that is known to probe macroscopic quantities of CNTs, is welcome.

Figure 8 shows the diameter distributions for ethanol-grown CNTs comparing electron diffraction data to Raman spectroscopy data. Specifically, the intensity ratio of the radial breathing mode (RBM) to G-line was used as a measure of the populations of CNTs according to their diameter. Between 0.9 and 1.2 nm diameters the Raman data concurs with the electron diffraction data - both show a rising population of CNTs. However, the Raman data suggests that, relative to the 1.0 nm diameter CNTs, there are between five and nine times as many CNTs in the 1.5-1.6 nm diameter range (for the 633 and 753 nm laser wavelength respectively). The 1.6-to-1.0 nm population ratio for electron diffraction is nearer unity (Figure 8). This suggests that, either electron diffraction was sampling smaller members of the parent CNT population or the Raman RBM:G line intensity ratio overestimates the larger CNT populations (He *et al* also observe this slight discrepancy between distributions[30]). We are inclined to believe the latter for the following three reasons.

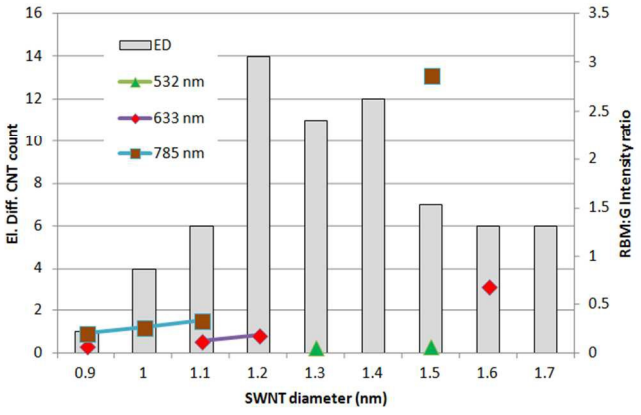

Figure 8. Carbon nanotube counts measured using electron diffraction (ED) of *individual* tubes compared to the Raman signal from *macroscopic quantities* of tubes by three different laser excitation energies (coloured symbols). See the Supplementary Information for experimental details.

First, the Raman differential cross section of a CNT shows a near ten-fold variation, 30 to 300 barns sr^{-1}, and is specific to the tube type[38]. In effect, bigger tubes scatter more light than thinner tubes.

Second, the RBM excitation is mediated by the dielectric response of the electron gas within the CNT to the electric field of the laser. Therefore, the near-resonant condition of the laser energy to inter-band transitions (E_{jj}) for certain CNT chiralities, selectively enhances some RBMs over others[39,40]. Because the RBM mode indirectly couples to the laser via a photon-exciton-phonon mechanism, it is sensitive to both the photon-exciton matrix elements (which shows a monotonic trend with CNT diameter) and the exciton-phonon matrix elements, which are highly chiral sensitive and do not show a monotonic variation with diameter[41].

Third, the RBM frequency tends to shift slightly with the extent of bundling[42] making unique CNT diameter identification particularly hazardous, especially towards the larger diameters where many chiralities (and interband transitions, E_{jj}) are compatible with the data. CNT population statistics rarely venture beyond 1.6 nm diameter because of this ambiguity[40,43,44]. Photoluminescence excitation (PLE) is significantly better for chiral indexing of CNTs[8,45-47], but the requirement of a band-gap renders approximately one third of the CNTs invisible.

The nature of CNTs grown with different precursors

Our survey of the structural properties of CNTs grown with different carbon precursors behaved similarly to that conducted by He *et al*[30] and can be understood within existing frameworks. First, the CNT diameter distribution (Figure 5) and SWNT yield is dictated by the size of the iron particles at the point in time (and temperature) where the carbon precursor starts to pyrolyse. The relationship may not be definitive[19], but there is compelling evidence that, under slow growth conditions where thermodynamic equilibrium is maintained, there is a close size relationship between the size of a catalytic particle and the diameter of the CNT it nucleates[7,17-19]. While we have *not* seen catalytic iron particles inside the CNTs that prove this (Hoecker *et al* have recently put forward an explanation for this apparent absence[48]), it is reasonable to assume that the small mean and variance in CNT diameters grown with ethanol and

View Article Online
DOI: 10.1039/C6NR03895F

toluene are due to small (2 to 3 nm) iron particles with a narrow distribution. Using a hydrocarbon with a higher pyrolysis temperature nucleates CNTs on bigger, wider distributions of iron particles – 3 to 6 nm for methane (Figure 6). The large DWNT yield of methane (73%) concurs with this interpretation[17,20]. Thus CNT diameter and SWNT/DWNT selectivity is accomplished, to a certain extent, by the combination of pyrolytic temperature differences between ferrocene, ethanol, toluene and methane, and the strong temperature gradient that provides a narrow time window to (Ostwald) ripen the iron clusters sufficiently *and* raise the temperature quickly to proceed to rapid CNT growth at the highest temperature in the bulk of the furnace, i.e. this is a matter of pyrolytic timing and temperature matching. The role of hydrogen as the carrier gas was crucial too, because the reducing atmosphere prevents amorphous carbon formation and promotes hydrogen abstraction from the hydrocarbon precursors at lower temperature. As an aside, it is worth pointing out that circumventing the ripening of iron clusters in a hot gas has been tried with spark-produced iron clusters with limited success[49]. Small, size-selected catalytic nano-particles that do not ripen at high temperature requires a significantly more sophisticated fabrication method, e.g. cluster beams[50,51].

Second, the chiral angle distribution (Figure 6) shows the same variation as He *et al* for CO (strong arm-chair bias) and methane (flatter variation) for chirality[30], which can be understood to be dictated by the temperature of the iron particle at CNT nucleation[52-55]. According to Artyukov *et al*, at low temperatures (ethanol & toluene) the nucleation mechanism is controlled by contact free-energy between the CNT and catalyst, which favours CNTs with near armchair or zig-zag configurations[53]. However, Hedman *et al* argues that the thermodynamic stability of the tube dictates the chirality[54], but fails to explain the preponderance of near-armchair *(n,n-1)* type CNTs typically seen in experiments[9,11,29,32,43,44,46]. In the model proposed by Artyukov *et al*[53], a strong bias towards armchair-type CNTs for ethanol (armchair: zig-zag = 7:1) and toluene (3:1), crudely translates, via the Boltzmann factor, into activation temperatures of ~260 ^{o}C (ethanol) and ~680 ^{o}C (toluene). This assumes that the 90 meV contact free-energy difference between zig-zag and armchair interfaces determined for nickel and cobalt, holds for iron too (See Figure 2(a) in Artyukov *et al*[53]). However, this simple comparison ignores the reactive influence of hydroxyl radicals, which are known to facilitate growth by etching amorphous carbon[56], and oxygen which has been implicated in high densities of defect formation[26]. Further, small amounts of ammonia added to a CO and CO_2 precursor mix has been found to select the chiral angle in preference for armchair CNTs[57]. However, a reduced CNT yield resulted, suggesting that etching was the main selection mechanism.

The flatter chirality distribution for methane can be understood to be a consequence of the kinetically-limited growth regime at higher temperature. Artyukov *et al* predict the highest growth rate for (*n,n/2*) CNTs, with a chiral angle of 19.1^{o} and the broad peak we observe in the 15^{o} to 20^{o} bin (figure 6) concurs with this[53].

Least understood is, perhaps, the nature of the small fraction of DWNTs grown with toluene. Two aspects of these tubes stand out. First, the unusually small distance between inner and outer CNTs (0.286 nm) is significantly smaller than that for methane (0.384 nm) and still well below the c/2 spacing for graphite (0.334 nm)[2]. To date, the smallest inter-tube distance reported for a DWNT is 0.31 nm.[58] Second, the excess number of DWNTs seen with a chiral angle change of -15^{o} to -20^{o}, going from the inner CNT to the outer CNT, is very suggestive and it is worth speculating how this particular correlation might arise.

The pyrolysis of toluene creates a wealth of hydrocarbons at both low and high pressures[59,60] with a broad range of molecular fragments. Likewise, we have observed the full set of molecular fragments, C_1, C_2, …C_6, using mass spectroscopy of toluene pyrolysed in our reactor when hydrogen is used, but not for nitrogen[61]. This is consistent with other observations where hydrogen was seen to be crucial for SWNT formation and hydrogen abstraction from the precursor[62,63]. Hydrogen abstraction of toluene creates a benzyl radical, one of the first pyrolytic products[59]. However, a small fraction of the benzyl radical reconfigures its bonding arrangement to form a 5-fold ring (PC12 in Zhang *et al*[59]) which, by further hydrogen abstraction, forms of 5-ethenylidene-1,3-cyclopentadiene (PC13, C_7H_6 , molar fraction ~10^{-4} at 1200^{o}C). This may be regarded as a 5-fold ring double-bonded to an ethene fragment. The catalytic surface may then facilitate the bond scission between C_2 and C_3 because of the energetic stabilization of C-dimers and sub-surface carbon concentration[64,65], which then provides ready molecular fragments to incorporate into the nascent CNT. Incorporation of a 5-fold ring into the tube has two effects: if the 5-fold ring goes into the outer tube, the negative curvature forces the outer tube to close onto the inner CNT. The elastic strain energy of the defect will drive the rapid healing of the 5-fold rings by forming a 7-fold ring behind it at the catalyst-tube boundary[66]. This 5-7 defect allows the outer tube to change chirality, depending on the orientation of the 5-7 defect[66]. Even with a small molar fraction of 5-fold molecular ring fragments, the incorporation of multiple 5-7 defects may allow the inner and outer CNT chiralities to diverge. At first sight, this seems problematic, because the number of kink sites ("cosy corners" – Ding *et al*[52]) onto which carbon atoms dock is proportional to the chiral angle[52,67]. If the outer tube has a lower chiral angle than the inner (as we observe), then the outer tube must incorporate more carbon atoms (per kink site) than the inner tube. Given the 7 DWNTs seen for toluene with a large negative $\Delta\alpha$, with an average chiral angles of 4.3^{o} (outer) and 26.3^{o} (inner), the carbon atom per kink site, yields a ratio of 6:1 outer to inner. If the DWNT can grow with this incorporation ratio per kink site, then the two walls of the DWNT can grow together. Substantial mechanical (and electronic) coupling should then exist between the inner and outer tubes[68,69]. The persistence of these structural links may require the absence of water, hydroxyls and oxygen to prevent

View Article Online
DOI: 10.1039/C6NR03895F ARTICLE

the outer tubes from 'opening up' to a more conventional inter-tube distance. CNT growth with phenol as a carbon precursor would be an effective test of this hypothesis. However, if tight inter-tube distances can be replicated, they offer a chance to create tube with unusual electronic and mechanical properties[68].

Conclusion

We find that ethanol and toluene are an effective carbon source for narrow single-walled carbon nanotubes with near 90 % yields with a strong bias towards armchair chiralities. These are selected by thermodynamic properties of the CNT-metal particle contact free energy. While DWNTs are rare, those produced with toluene show evidence of unusually narrow inter-tube distances. Methane produces primarily double-walled nanotubes with an intermediate chirality favoured by the fastest kinetic growth rates in the kinetically-limited regime. The differences in growth regimes suggest that some degree of control of coupling between inner and outer CNTs in DWNTs may be possible at the point at which growth starts.

Acknowledgements

CP and KK thank the European Commission for the funding of the project under the Seventh Framework Programme FP7/2007-201, ERC grant agreement number 259061.

Notes and references

[a] Department of Materials Science & Metallurgy, University of Cambridge, 27 Charles Babbage Road, Cambridge CB3 0FS, United Kingdom.

Electronic Supplementary Information (ESI) available: [details of any supplementary information available should be included here]. See DOI: 10.1039/b000000x/

1 M.S. Dresselhaus, G. Dresselhaus and P.C. Eklund, *Science of Fullerenes and Carbon Nanotubes*, 1996, Academic Press, San Diego.
2 P.J.F. Harris, *Carbon Nanotube Science*, 2011, Cambridge University Press, Cambridge.
3 G.G. Tibbetts, D.W. Gorkiewicz and R.L. Alig, *Carbon*, 1993, **31**(5), 809-814.
4 M.S. Dresselhaus, G. Dresselhaus, K. Sugihara, I.L. Spain, H.A. Goldberg and M. Cardona (Ed), *Carbon Fibers and Filaments*, 1988, Springer Series in Mat. Sci, Springer-verlag, Berlin.
5 V. Jourdain and C. Bichara, *Carbon*, 2013, **58**, 2-39.
6 P. Nikolaev, M.J. Bronikowski, R. K. Bradley, F. Rohmund, D.T. Colbert, K.A. Smith and R.E. Smalley, *Chem. Phys. Lett.*, 1999, **313**, 91-97.
7 H. Dai, A.G. Rinzler, P. Nikolaev, A. Thess, D.T. Colbert and R.E. Smalley, *Chem. Phys. Lett.*, 1996, **260**, 471-475.
8 S.M. Bachilo, L. Balzano, J.E. Herrera, F. Pompeo, D.E. Resasco and R.B. Weisman, *J. Am. Chem. Soc.*, 2003, **125**, 11186-11187.
9 B. Wang, C.H.P. Poa, L. Wei, L.-J. Li, Y. Yang and Y. Chen, *J. Am. Chem. Soc.*, 2007, **129**, 9014-9019.
10 J.E. Herrera, L. Balzano, A. Borgna, W.E. Alvarez and D.E. Resasco, *J. Catalysis*, 2001, **204**, 129-145.
11 M. He, A.I. Chernov, P.V. Fedotov, E.D. Obraztsova, J. Sainio, E. Rikkinen, H. Jiang, Z. Zhu, Y. Tian, E.I. Kauppinen, M. Niemelä and A.O.I. Krause, *J. Am. Chem. Soc.*, 2010, **132**, 13994-13996.
12 F. Yang, X. Wang, D. Zhang, J. Yang, D. Luo, Z. Xu, J. Wei, J.-Q. Wang, Z. Xu, F. Peng, X. Li, R. Li, Y. Li, M. Li, X. Bai, F. Ding and Y. Li, *Nature*, 2014, **510**, 522-524.
13 J. R. Sanchez-Valencia, T. Dienel, O. Gröning, I. Shorubalko, A. Mueller, M. Jansen, K. Amsharov, P. Ruffieux and R. Fasel, *Nature*, 2014, **512**, 61-64.
14 J. Liu, C. Wang, X. Tu, B. Liu, L. Chen, M. Zheng, and C. Zhou, *Nat. Comms.*, 2012, **3**, 1-7.
15 R.T.K. Baker, P.S. Harris, R.B. Thomas and R.J. Waite, *J. Catalysis*, 1973, **30**, 86-95.
16 S. Iijima, *Nature*, 1991, **354**, 56.
17 E. Lamouroux, P. Serp and P. Kalck, *Cat. Rev.*, 2007, **49**, 341-405.
18 A.G. Nasibulin, P.V. Pikhitsa, H. Jiang and E.I. Kauppinen, *Carbon*, 2005, **43**, 2251-2257.
19 M.-F.C. Fiawoo, A.-M. Bonnot, H. Amara, C. Bichara, J. Thibault-Pénisson and A. Loiseau, *Phys. Rev. Lett.*, 2012, **108**, 195503
20 S. Helveg, C. López-Cartes, J. Sehested, P.L. Hansen, B.S. Clausen, J.R. Rostrup-Nielsen, F. Abild-Pedersen and J.K. Nørskov, *Nature*, 2004, **427**, 426-429.
21 S. Hofmann, R. Sharma, C. Ducati, G. Du, C. Mattevi, C. Cepek, M. Cantoro, S. Pisana, A. Parvez, F. Cervates-Sodi, A.C. Ferrari, R. Dunin-Borkowski, S. Lizzit, L. Petaccia, A. Goldoni and J. Robertson, *Nano Lett.*, 2007, **7** (3), 602-608.
22 M. Lin, J.P.Y. Tan, C. Boothroyd, K.P. Loh and Y.-L. Foo, *Nano Lett.*, 2007, **7** (8), 2234-2238.
23 A.J. Page, Y. Ohta, S. Irle and K. Morokuma, *Acc. Chem. Res.*, 2010, **43** (10), 1375-1385.
24 A. Moisala, A.G. Nasibulin, D.P. Brown, H. Jiang, L. Khriachtchev and E.I. Kauppinen, *Chem. Eng. Sci.*, 2006, **61**, 4393-4402.
25 J. Kong, A.M. Cassell and H. Dai, *Chem. Phys. Lett.*, 1998, **292**, 567-574.
26 W. Ren, F. Li, J. Chen, S. Bai and H.-M. Cheng, *Chem. Phys. Lett.*, 2002, **359**, 196-202.
27 S. Maruyama, R. Kojima, Y. Miyauchi, S. Chiashi and M. Kohno, *Chem. Phys. Lett.*, 2002, **360**, 229-234.
28 Y. Tian, Z. Hu, Y. Yang, X. Wang, X. Chen, H. Xu, Q. Wu, W. Ji and Y. Chen, *J. Am. Chem. Soc.*, 2004, **126**, 1180-1183.
29 G. Lolli, L. Zhang, L. Balzano, N. Sakulchaicharoen, Y. Tan and D. E. Resasco, *J. Phys. Chem. B.*, 2006, **110**, 2108-2115.
30 M. He., H. Jiang, E.I. Kauppinen and J. Lehtonen, *Nanoscale*, 2012, **4**, 7394-7398.
31 C. Paukner and K. K. K. Koziol, *Sci. Rep.*, 2014, **4**, 3903.
32 K. Hirahara, M. Kociak, S. Bandow, T. Nakahira, K. Itoh, Y. Saito and S. Iijima, *Phys. Rev. B.* 2006, **73**, 195420.
33 C.S. Allen, C. Zhang, G. Burnell, A.P. Brown, J. Robertson and B.J. Hickey, *Carbon*, 2011, **49**, 4961-4971.
34 B.W. Smith and D.E. Luzzi, *J. Appl. Phys.*, 2001, **90**, 3501.

View Article Online
DOI: 10.1039/C6NR03899F

35 Z. Liu, Q. Zhang and L.-C. Qin, *Appl. Phys. Lett.*, 2005, **86**, 191903.
36 H. Jiang, A.G. Nasibulin, D.P. Brown and E.I. Kauppinen, *Carbon*, 2007, **45**, 662-667.
37 D.L. Dorset, *Structural Electron Crystallography*, 1995, Springer, Berlin.
38 J.E. Bohn, P.G. Etchegoin, E.C.L. Ru, R. Xiang, S. Chiashi and S. Maruyama, *ACS Nano*, 2010, **4** (6), 3466-3470
39 H. Kataura, Y. Kumazawa, Y. Maniwa, I. Umezu, S. Suzuki, Y. Ohtsuka and Y. Achiba, *Synth. Metals*, 1999, **103**, 2555-2558.
40 J. Maultzsch, H. Telg, S. Reich and C. Thomsen, *Phys. Rev. B.*, 2005, **72**, 205438.
41 K. Sato, R. Saito, A.R.T. Nugraha and S. Maruyama, *Chem. Phys. Lett.*, 2010, **497**, 94-98.
42 Z. Zhang, E. Einarsson, Y. Murakami, Y. Miyauchi and S. Maruyama, *Phys. Rev. B.*, 2010, **81**, 165442.
43 R. Rao, D. Liptak, T. Cherukuri, B.I. Yakobson and B. Maruyama, *Nat. Mat.*, 2012, **11**, 213-216.
44 M. Fouquet, B.C. Bayer, S. Esconjauregui, R. Blume, J.H. Warner, S. Hofmann, R Schlögl, C. Thomsen and J. Robertson, *Phys. Rev. B.*, 2012, **85**, 235411.
45 M.J. O'Connell, S.M. Bachilo, C.B. Huffman, V.C. Moore, M.S. Strano, E.H. Haroz, K.L. Rialon, P.J. Boul, W.H. Noon, C. Kittrell, J. Ma, R.H. Hauge, R.B. Weisman and R.E. Smalley, *Science*, 2002, **297**, 593-596.
46 H. Wang, L. Wei, F. Ren, Q. Wang, L.D. Pfefferle, G.L. Haller and Y. Chen, *ACS Nano*, 2013, **7** (1), 614-626
47 Y. Miyauchi, S. Chiashi, Y. Murakami, Y. Hayashida and S. Maruyama, *Chem. Phys. Lett.*, 2004, **387**, 198-203.
48 C. Hoecker, F. Smail, M. Bajada, M. Pick and A. Boies, *Carbon*, 2016, **96**, 116-124.
49 K. Mustonen, P. Laiho, A. Kaskela, Z. Zhu, O. Reynaud, N. Houbenov, Y. Tian, T. Susi, H. Jiang, A.G. Nasibulin and E. I. Kauppinen, *Appl. Phys. Lett.*, 2015, **107**, 013106
50 P.R. Ellis, C.M. Brown, P.T. Bishop, J. Yin, K. Cooke, W.D. Terry, J. Liu, F. Yin and R.E. Palmer, *Faraday Discuss*, 2016, **188**, 39-56
51 R.E. Palmer (2016) private communication
52 F. Ding, A.R. Harutyunyan and B.I. Yakobson, *PNAS*, 2009, **106** (8), 2506-2509.
53 V. I. Artyukov, E.S. Penev and B.I. Yakobson, *Nat. Comms.*, 2014, **5**, 1-6.
54 D. Hedman, H.R. Barzegar, A. Rosen, T. Wågberg and J.A. Larsson, *Sci. Rep.*, 2015, **5**, 16850.
55 H. Dumlich and S. Reich, *Phys. Rev. B.*, 2010, **82**, 085421.
56 D.N. Futaba, J. Goto, S. Yasuda, T. Yamada, M. Yumura and K. Hata, *Adv. Mater.*, 2009, **21**(47), 4811-4815.
57 Z. Zhu, H. Jiang, T. Susi, A.G. Nasibulin and E.I. Kauppinen, *J. Am. Chem. Soc.*, 2011, **133**, 1224-1227
58 F. Villalpando-Paez, H. Son, D. Nezich, Y.P. Hsieh, J. Kong, Y.A. Kim, D. Shimamoto, H. Muramatsu, T. Hayashi, M. Endo, M. Terrones and M.S. Dresselhaus. *Nano Lett.*, 2008, **8** (11), 3879-3886.
59 T. Zhang, L. Zhang, X. Hong, K. Zhang, F. Qi, C.K. Law, T. Ye, P. Zhao and Y. Chen, *Comb. & Flame*, 2009, **156**, 2071-2083.
60 M.B. Colket and D.J. Seery, *Symposium (International) on Combustion*, 1994, **25**(1), 883-891.
61 C. Paukner, *PhD Thesis*, University of Cambridge, 2015.
62 Y.-Q. Xu, E. Flor, H. Schmidt, R.E. Smalley and R.H. Hauge, *Appl. Phys. Lett.*, 2006, **89**, 123116
63 B. Shukla,, T. Saito, M. Yumura and S. Iijima, *Chem. Commun.*, 2009, **2009**, 3422-3424
64 M. Moors, H. Amara, T.V. de Bocarmé, C. Bichara, F. Ducastelle, N. Kruse and J.-C. Charlier, *ACS Nano*, 2009, **3** (3), 511-516.
65 H. Amara, C. Bichara and F. Ducastelle, *Phys. Rev. Lett.*, 2008, **100**, 056105.
66 Q. Yuan, Z. Xu, B.I. Yakobson and F. Ding, *Phys. Rev. Lett.*, 20012, **108**, 245505.
67 S. Reich, L. Li and J. Robertson, *Phys. Rev. B*, 2005, **72**, 165423.
68 S. Hai-Yang, L. Li-Feng, and F. Feng, *J. Phys. D: Appl. Phys*, 2009, **42**, 055414.
69 O. V. Kharissova and B. I. Kharisov, *RSC Adv.*, 2014, **4**, 30807.